


Article

# Syntheses, Structures, and Characteristics of Three Metal Complexes Constructed Using Hexacarboxylic Acid

Lingshu Meng, Lun Zhao \* , Guanlin Guo, Xin Liu, Zhijun Liang, Jian Xiu and Xu Zhou

College of Chemistry, Changchun Normal University, Changchun 130032, China

\* Correspondence: zhaolun7511@126.com; Tel.: +86-431-86168903

Received: 25 October 2019; Accepted: 2 December 2019; Published: 4 December 2019



**Abstract:** In this study, three new 3D coordination polymers (CPs),  $\{[\text{Cd}_3(\text{L})(\text{H}_2\text{O})_6]\cdot\text{H}_2\text{O}\}_n$  (**1**),  $\{[\text{Cu}_{1.5}(\text{L})_{0.5}(\text{bimb})_{1.5}]\cdot 5\text{H}_2\text{O}\cdot\text{DMF}\}_n$  (**2**), and  $\{[\text{Mn}_{1.5}(\text{H}_3\text{L})(\text{bibp})_{0.5}(\text{H}_2\text{O})_2]\cdot 3\text{H}_2\text{O}\}_n$  (**3**) (*bimb* = 1,3-bis(imidazol-1-yl)benzene, *bibp* = 1,4-bis((4-imidazol-1-yl)benzyl)piperazine), were prepared under solvothermal or hydrothermal conditions based on a hexadentate ligand (1,3,5-triazine-2,4,6-triamine hexa-acetic acid ( $\text{H}_6\text{L}$ )). Structural elucidations were carried out by IR spectra along with single-crystal X-ray diffraction analysis, while thermogravimetric analysis (TGA) (dynamic and isothermal) and XRD techniques were used for property evaluations of the polymers. Furthermore, the fluorescence properties and detection of the  $\text{Fe}^{3+}$  ions in **1** were tested at room temperature, and the electrochemical behavior of **2** is also stated in this article.

**Keywords:** coordination polymers; hexacarboxylic acid; fluorescent probe; electrochemical behaviors

## 1. Introduction

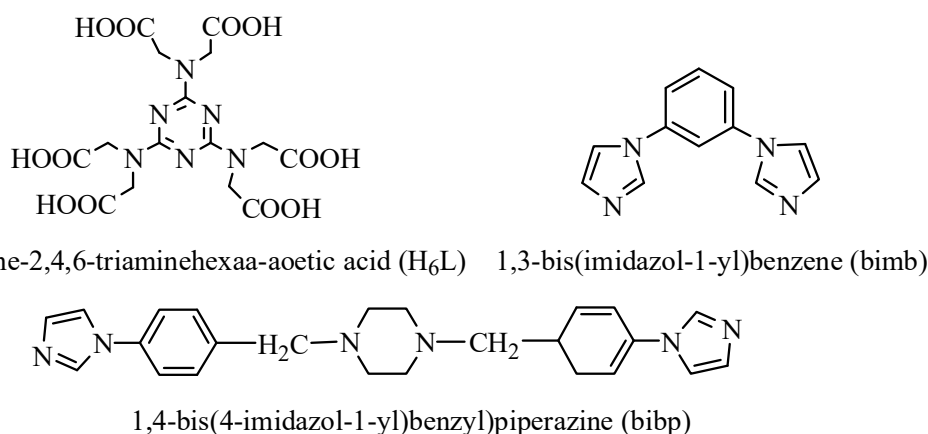
With special pore structures and potential application values, coordination polymers (CPs) over the past few decades have attracted researchers' interest [1–15]. Recently, researchers have found some specially structured CPs that possess characteristic high-intensity fluorescence shooting, which could be applied to pollution object detection by contrasting fluorescent signals in different states. The detection method had high sensitivity, a fast detection speed, and the advantages of easy operation. Currently, the literature reports on the benefits of using this property to detect metal ions, aromatic nitro compounds, and other small molecules [16–22].

It is well known that  $\text{Fe}^{3+}$  is an indispensable trace element in the human body, playing a vital role in oxide reductase catalysis, DNA synthesis, and oxygen transport and storage [23–29]. A lack of  $\text{Fe}^{3+}$  might be because of anemia or heart failure, and an excess of it may damage the liver. These diseases are all serious; however, it has been reported that some CPs can selectively perceive  $\text{Fe}^{3+}$  [30–32]. For now, it is still necessary to synthesize CPs with higher selectivity and sensitivity, so much work needs to be done.

Furthermore, with the development of the global economy and the rapid growth of the world's population, the demand for energy is also growing. Electric energy is one of the most important energy sources in people's lives:  $\text{Co}^{2+}$ ,  $\text{Cu}^{2+}$ , and  $\text{Ni}^{2+}$  plasmas have good redox activity as the central metal ions of complexes. At the same time, bulk-modified carbon paste electrodes do not dissolve in water and common organic solvents, so they are suitable electrodes for research.

Because of the diversity of coordination, hexacarboxylic acid could react with transition metal ions and nitrogen-containing ligands to form a variety of spatial topologies. Li and colleagues designed and synthesized two new CPs using 1,3,5-triazine-2,4,6-triamine hexa-acetic acid, and both coordination polymers had very high sensitivity to sensing properties at very low concentrations

of nitro derivatives [33]. Song and coworkers synthesized three new coordination polymers with  $H_6L$  and different ligands and indicated that these compounds displayed high-sensitivity luminescent sensing functions for nitrobenzene. Additionally, surface photovoltage spectroscopy and electric-field-induced surface photovoltage spectroscopy showed that these compounds could behave as *p*-type semiconductors [34]. Cd complexes have good luminescent properties, and they are widely used in fluorescence sensing [35]. Cu and Mn complexes have been widely reported in the fields of catalysis, magnetism, and electrochemistry [36,37]. In this work, three different metal ion complexes were synthesized under hydrothermal/solvothermal conditions using hexacarboxylic acid and two kinds of ligands (Scheme 1): they were named  $\{[Cd_3(L)(H_2O)_6] \cdot H_2O\}_n$  (1),  $\{[Cu_{1.5}(L)_{0.5}(bimb)_{1.5}] \cdot 5H_2O \cdot DMF\}_n$  (2), and  $\{[Mn_{1.5}(H_3L)(bibp)_{0.5}(H_2O)_2] \cdot 3H_2O\}_n$  (3). They were fully characterized by thermogravimetric analysis (TGA), IR spectra, photoluminescence, elemental analysis, and single-crystal X-ray diffraction analysis. These three complexes exhibited good 3D structure, and fluorescence titrations confirmed that 1 showed excellent potential in sensing  $Fe^{3+}$  in water. Moreover, the electrochemical properties of 2 were investigated by means of cyclic voltammetry.



**Scheme 1.** Molecular structure of several ligands.

## 2. Experimental Section

### 2.1. Materials and Methods

All solvents and reagents for synthesis were of reagent grade quality, were bought from commercial sources, and were used as received. The ligands  $H_6L$ , bibp, and bimb were purchased from Jinan Henghua Sci. & Tec. Co. Ltd. (in Shandong Province, China). Powder X-ray diffraction (PXRD) patterns were collected on a D2 PHASER A26-X1 XRD diffractometer. IR spectra ( $4000\text{--}400\text{ cm}^{-1}$ ) were obtained from KBr pellets with an FTIR Nexus spectrophotometer. Elemental analyses were performed on a Perkin-Elmer 240 C analyzer. Thermogravimetric analysis (TGA) curves were measured under an air atmosphere at a heating rate of  $10\text{ }^\circ\text{C}/\text{min}$  on a Perkin-Elmer TG-7 thermal analyzer. The fluorescence spectra were carried out on a HITACHI F-7000 Spectrometer. Electrochemical properties were studied on a DF-2002 electrochemical workstation [38].

### 2.2. Synthesis of $\{[Cd_3(L)(H_2O)_6] \cdot H_2O\}_n$ (1)

A mixture of  $Cd(NO_3)_2 \cdot 4H_2O$  (30.8 mg, 0.1 mmol), 4-(imidazol-1-ylmethyl)benzonitrile (18.3 mg, 0.1 mmol)(auxiliary agent), and  $H_6L$  (47.4 mg, 0.1 mmol) were dissolved in  $H_2O$  solvent (10 mL). After being mixed evenly, it was placed in a Parr Teflon-lined stainless steel vessel (20 mL) and heated at  $160\text{ }^\circ\text{C}$  for 72 h under autogenous pressure. Colorless crystals were acquired. The reaction yield was ca. 60% based on an  $H_6L$  ligand. The elemental analysis for  $C_{15}H_{26}Cd_3N_6O_{19}$ (%): C, 19.34; H, 2.81; N, 9.02. Found: C, 19.71; H, 2.89; N, 8.86. FT-IR ( $4000\text{--}400\text{ cm}^{-1}$ ): 3214 (m), 1570 (w), 1483 (w), 1440 (w), 1197 (m), 1180 (s), 986 (s), 818 (s), 719 (m).

### 2.3. Synthesis of $\{[Cu_{1.5}(L)_{0.5}(bimb)_{1.5}] \cdot 5H_2O \cdot DMF\}_n$ (2)

A mixture of  $Cu(NO_3)_2 \cdot 3H_2O$  (24.2 mg, 0.1 mmol), bimb ligand (21.1 mg, 0.1 mmol), and  $H_6L$  (47.4 mg, 0.1 mmol) were dissolved in DMF/ $H_2O$ /0.1M $HNO_3$  solvent (8:2:1, 11 mL). After being mixed evenly, it was placed in a Parr Teflon-lined stainless steel vessel (20 mL) and heated at 80 °C for 72 h under autogenous pressure. Aquamarine crystals were acquired. The reaction yield was ca. 47% based on an  $H_6L$  ligand. The elemental analysis for  $C_{57}H_{64}N_{20}Cu_3O_{24}$ (%): C, 42.68; H, 4.02; N, 17.47. Found: C, 42.99; H, 4.12; N, 16.68. FT-IR (4000–400  $cm^{-1}$ ): 3736 (s), 3393 (s), 3130 (s), 1609 (m), 1517 (m), 1289 (m), 1250 (m), 1194 (s), 1113 (s), 988 (s), 811 (s), 792 (s).

### 2.4. Synthesis of $\{[Mn_{1.5}(H_3L)(bibp)_{0.5}(H_2O)_2] \cdot 3H_2O\}_n$ (3)

A mixture of  $MnCl_2 \cdot 4H_2O$  (19.7 mg, 0.1 mmol), bibp ligand (39.8 mg, 0.1 mmol), and  $H_6L$  (47.4 mg, 0.1 mmol) were dissolved in DMF/ $H_2O$ /0.1M $HNO_3$  solvent (8:2:1, 11 mL). After being mixed evenly, it was placed in a Parr Teflon-lined stainless steel vessel (20 mL) and heated at 80 °C for 72 h under autogenous pressure. Brown crystals were acquired. The reaction yield was ca. 51% based on an  $H_6L$  ligand. The elemental analysis for  $C_{54}H_{50}Mn_3N_{18}O_{34}$ (%): C, 39.12; H, 3.01; N, 15.22. Found: C, 39.07; H, 3.04; N, 15.19. FT-IR (4000–400  $cm^{-1}$ ): 3414 (s), 1552 (m), 1481 (s), 1315 (s), 1200 (m), 1062 (s), 988 (s), 855 (s), 809 (m).

### 2.5. X-ray Crystallography

Appropriate single crystals of compounds 1–3 were mounted on a glass fiber, and the intensity data were measured at 293 K on a Bruker SMART APEXII CCD area detector with graphite monochromatic Mo-K $\alpha$  radiation using the  $\omega$  scan mode ( $\lambda = 0.71073$  Å). Data reduction and cell refinement were performed with SADABS software packages. Absorption corrections were done using the empirical method, and all of the structures were solved with the direct method using SHELXS-97 [39]. The anisotropy of all nonhydrogen atoms determined their coordinates. The crystallographic data inferred and other relevant information about structural determination are shown in Table 1.

**Table 1.** Crystal data and structure refinement for 1, 2, and 3.

Compound	1	2	3
Molecular Formula	$C_{15}H_{26}Cd_3N_6O_{19}$	$C_{57}H_{64}N_{20}Cu_3O_{24}$	$C_{54}H_{50}Mn_3N_{18}O_{34}$
Formula weight	917.54	1593.85	1659.94
Crystal system	Monoclinic	Monoclinic	Triclinic
Space group	$P2_1/c$	$C2/c$	$P-1$
$a/\text{Å}$	9.7574 (3)	31.421 (3)	8.234 (2)
$b/\text{Å}$	15.1249 (5)	17.6474 (18)	10.610 (3)
$c/\text{Å}$	18.6267 (6)	17.2392 (17)	19.504 (6)
$\alpha/^\circ$	90	90	81.094 (6)
$\beta/^\circ$	95.449 (1)	117.491 (2)	87.935 (7)
$\gamma/^\circ$	90	90	86.408 (7)
$V/\text{nm}^3$	2736.50 (15)	8479.7 (15)	1679.6 (8)
Z	4	4	1
$D_c/(\text{g}\cdot\text{cm}^{-3})$	2.227	1.248	1.641
$F(000)$	1760	3260	847
$s$	1.090	1.189	1.039
$R_1/wR_2 [I > 2\sigma(I)]$	0.0235, 0.0623	0.1020, 0.3087	0.0682, 0.1824
$R_1/wR_2$ (all data)	0.0268, 0.0640	0.1684, 0.3611	0.1115, 0.2223

## 3. Results and Discussion

### 3.1. Structural Description of 1

CP 1 was crystallized in a monoclinic space group,  $P2_1/c$ , and it contained one carboxylic acid  $L^{6-}$  ligand, three crystallographically independent Cd(II) ions, six coordinated  $H_2O$  molecules, and

one free H<sub>2</sub>O molecule (Figure 1a). Each Cd(II) ion (Cd1, Cd2, and Cd3) had a distinct coordination environment. In detail, Cd 1 constituted a deformed octahedron with seven coordinates (coordination of Cd 1 with O1, O7, O8, O9, O10, OW1, and OW2); Cd 2 had a five-coordinate mode (coordination of Cd 2 with O1A, O2A, O3A, O6, and O12A); and Cd 3 had a six-coordinate mode (coordination of Cd 3 with O10, O11A, OW3, OW4, OW5, and OW6). In asymmetrical structural units, the six carboxylate groups of the ligand L<sup>6-</sup> exhibited four different bonding modes (Scheme 2). The distance of the Cd–O bond ranged from 2.186(2) to 2.537(2) Å. Adjacent Cd(II) ions were joined by carboxylic acid ligands L<sup>6-</sup> to form a 3D framework (Figure 1b). Using a topological approach, the carboxylic acid ligand L<sup>6-</sup> could be regarded as a 9-c node (Figure 1c) and the Cd(II) ion as a 3-c node or 4-c node (Figure 1d); therefore, the entire structure could be denoted by its topology (Figure 1e).

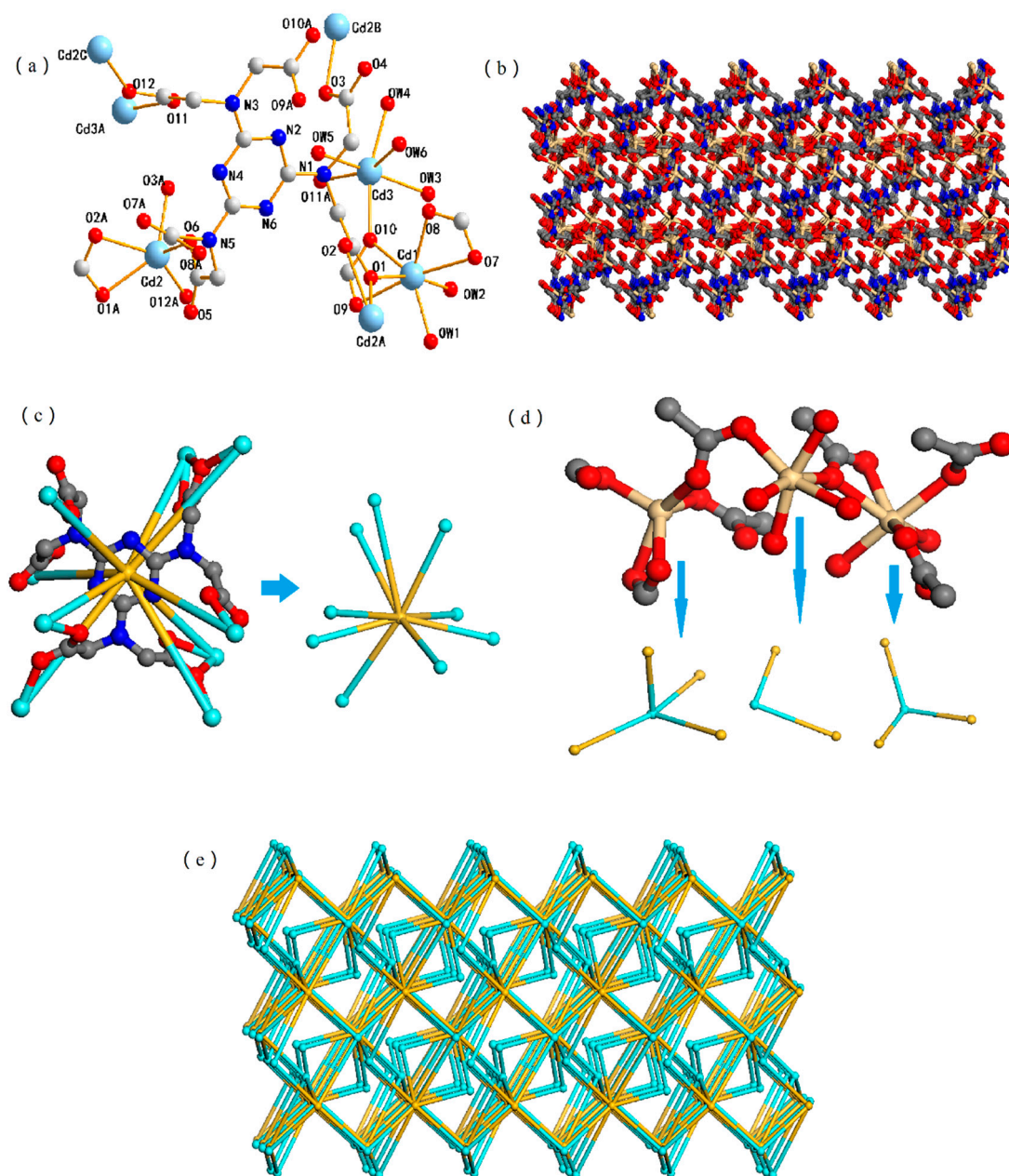
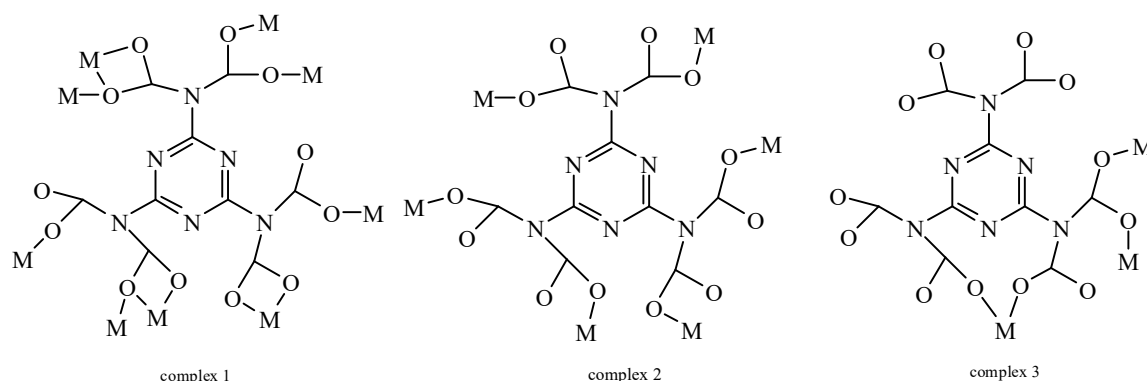


**Figure 1.** (a) The coordination environment for the three Cd(II) ions in **1**. (b) 3D framework with L<sup>6-</sup> and Cd(II) ions. (c) Nine-coordinate node of carboxylic acid L<sup>6-</sup>. (d) Three-coordinate node and four-coordinate node of Cd(II) ions. (e) 3D network topology representation of **1**.



**Scheme 2.** Coordination mode of carboxylic acid.

### 3.2. Structural Description of 2

CP 2 was crystallized in a monoclinic space group,  $C2/c$ , and it contained 3/2 bimb ligands, a 1/2 carboxylic acid  $L^{6-}$  ligand, 3/2 crystallographically independent Cu(II) ions, five uncoordinated  $H_2O$  molecules, and one free DMF molecule (Figure 2a). In asymmetrical structural units, the Cu(II) ions were four-connected by two oxygen atoms of  $L^{6-}$  ligands and two N atoms of bimb ligands, showing a distorted tetrahedron. Six carboxylate groups of the  $L^{6-}$  ligands exhibited a monodentate character (Scheme 2). The distance of the Cu–O bond ranged from 1.939(3) to 2.026(4) Å, and the Cu–N bond ranged from 1.975(5) to 2.021(5) Å. The Cu(II) ion was bonded to the carboxylic acid ligand  $L^{6-}$  to form a 3D framework structure (Figure 2b), and the bimb ligand was relinked to two carboxylic acid ligands of the  $L^{6-}$  ligand (Figure 2d) and populated into this 3D framework (Figure 2c). Using a topological approach, the carboxylic acid ligand  $L^{6-}$  and the Cu(II) ion could be regarded as a 6-c node and a 4-c node, respectively, and the ligand bimb could be regarded as a linker; therefore, the entire structure could be denoted by its topology (Figure 2e).

### 3.3. Structural Description of 3

CP 3 was crystallized in a triclinic space group  $P-1$ , and it contained 1/2 bimb ligands, one  $H_3L^{3-}$  ligand, 3/2 crystallographically independent Mn(II) ions, and five  $H_2O$  molecules (three uncoordinated and two coordinated) (Figure 3a). In asymmetrical structural units, two Mn(II) ions had different coordination environments; Mn1 was six-connected by two oxygen atoms of  $H_3L^{3-}$  ligands and four oxygen atoms of bound water; Mn2 was five-connected by four carboxylic oxygen atoms of  $H_3L^{3-}$  ligands and one N atom of bimb ligands; and two symmetrical Mn2 atoms formed a metal cluster, as shown in Figure 3b. Three carboxylate groups of the  $H_3L^{3-}$  ligands exhibited a monodentate character, leaving three uncoordinated (Scheme 2). The distance of the Mn–O bond ranged from 2.107(3) to 2.232(3) Å, and the Mn–N bond length was 2.145(3) Å. In this complex, the Mn(II) ion and  $H_3L^{3-}$  ligands formed 1D chains, and then the 1D chains formed into a 2D layer through bimb ligands (Figure 3b,c). The 3D frame was obtained by stacking the 2D layers. Using a topological approach, the Mn(II) ion (as a 3-c node) and the carboxylic acid ligand  $H_3L^{3-}$  could be regarded as a 3-c node; therefore, the entire structure could be denoted by its topology (Figure 3d).

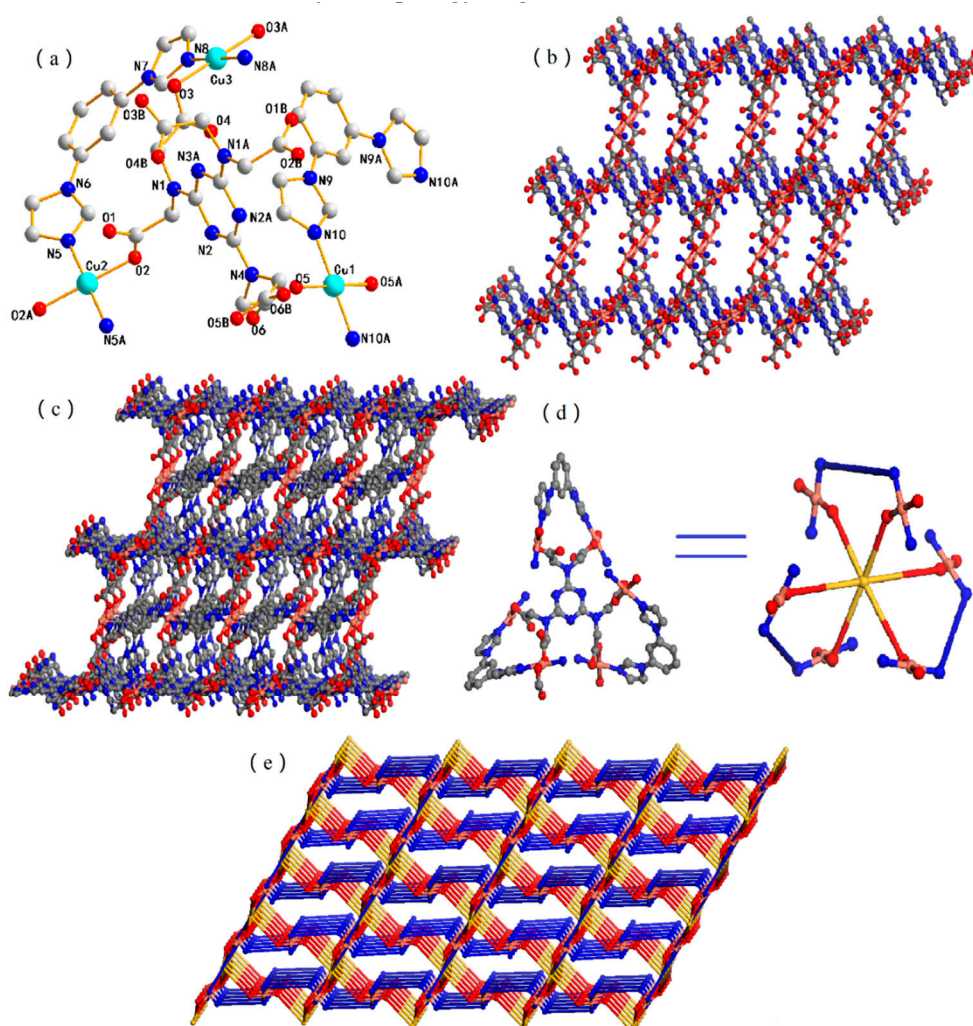


**Figure 2.** (a) The coordination environment for the three Cu(II) ions in **2**. (b) View of the 3D frame structure with  $L^{6-}$  and Cu(II) ions. (c) View of the 3D frame structure after it was filled with nitrogen-containing ligands. (d) View of a six-coordinate node and a four-coordinate node. (e) 3D network topology representation of **2**.

### 3.4. PXRD and Thermogravimetric Analysis (TGA)

The PXRD patterns for CPs **1**, **2**, and **3** were presented in Figures S1–S3 (in the Supplementary Information), respectively. The experimental data were in good agreement with the main peak of the corresponding simulations, proving their good phase purity.

TGA experiments were performed from 20 to 800 °C at a heating rate of 10 °C/min under an air atmosphere to evaluate the thermal stabilities of three complexes (Figure S4, in the ESI+). For **1**, the first phase of weight loss from 25 to 350 °C was caused by a release of  $H_2O$  molecules. Then, it continuously lost weight between 350 and 610 °C due to a collapse of the frameworks. The framework was stable up to ca. 610 °C. The final residue was CdO (obsd 45.23%, calcd 42.00%). For **2**, the first phase of weight loss from 25 to 160 °C was caused by a release of  $H_2O$  and DMF molecules (obsd 11.11%, calcd 10.16%). Then, it continuously lost weight between 160 and 450 °C, probably due to the thermal decomposition of ligand bimb and the collapse of the frameworks. The framework was stable up to ca. 450 °C. The final residue was CuO (obsd 15.01%, calcd 14.88%). For **3**, the first phase of weight loss from 25 to 105 °C was caused by a release of  $H_2O$  molecules (obsd 8.78%, calcd 5.42%), and the framework began to decompose between 240 and 430 °C. The final residue was MnO (obsd 13.49%, calcd 12.82%).

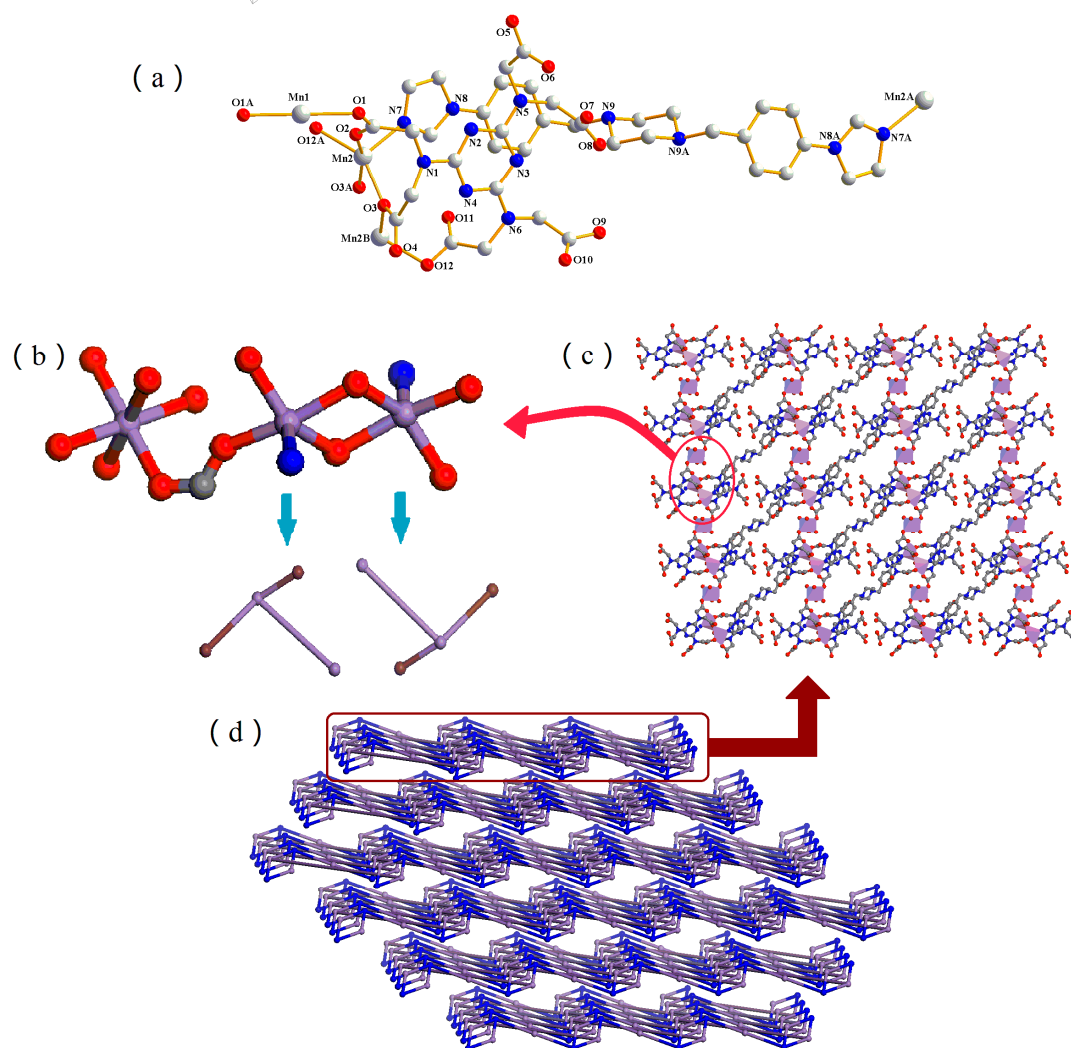


**Figure 3.** (a) The coordination environment for the three Mn(II) ions in **3**. (b) View of the Mn(II) ion coordination mode. (c) View of the 2D frame structure. (d) 3D network topology representation of **3**.

### 3.5. Photoluminescent Properties of **1**

The solid complex **1** and the ligand were subjected to a fluorescence test at room temperature, and the resulting spectrum is shown in Figure 4. At a maximum emission wavelength of 300 nm, **1** had an emission peak at 374 nm, and the maximum emission peak of the hexacarboxylic acid  $H_6L$  ligand was at 383 nm at an excitation wavelength of 321 nm. Since the central metals of **1** were Cd(II) ions, which are not easily oxidized or reduced in the skeleton due to the outermost electron arrangement, there was a stable  $d^{10}$  configuration [40,41]. For complex **1**, the emissions could be essentially ascribed to the luminescence of the carboxylic acid ligand  $H_6L$ , since a similar emission was observed in the free  $H_6L$  ligand. The fluorescence emission peak of **1** at 374 nm ( $\lambda_{ex} = 300$  nm) produced a small blue shift at 383 nm ( $\lambda_{ex} = 321$  nm) relative to the ligand  $H_6L$ , which was mainly due to the coordination of the ligands with the metals.

### 3.6. Detection of $Fe^{3+}$ Ions

Through the literature, we discovered a fluorescence sensing experiment of  $Fe^{3+}$  with good effects on quenching. First, 2 mL of aqueous solvent suspensions containing the crystal samples of **1** (2 mg) were subjected to an ultrasound for half an hour. Next,  $Fe(NO_3)_3$  ( $0.2 \text{ mmol}\cdot\text{L}^{-1}$  (mM)) was gradually added, and the luminescence intensity was tested. As is depicted in Figure 5a, the fluorescence

intensities of the  $\text{Fe}^{3+}$  stable suspensions of **1** were quenched gradually, decreasing as the concentration of  $\text{Fe}^{3+}$  increased, and the quenching efficiency was 87.63% when the  $\text{Fe}^{3+}$  concentrations rose to 0.1111 mM. The quenching consequent could be rationalized by the Stern–Volmer equation quantitatively:  $I_0/I = K_{sv}[M] + 1$  ( $I_0$  and  $I$  are the luminescence intensities of **1** without and with the addition of an analyte, respectively,  $K_{sv}$  is the quenching constant, and  $[M]$  is the molar concentration of  $\text{Fe}^{3+}$ ) [42].  $K_{sv}$  was calculated to be  $1.56 \times 10^4 \text{ M}^{-1}$  from the Stern–Volmer plots (Figure 5b), and it showed a good linear relationship when the concentration was low (0.0039–0.0206 mM). The PXRD data of complex **1** in aqueous solution and  $\text{Fe}^{3+}$  solution showed its stability in solution (Figure S2 in the ESI<sup>†</sup>). Then, the UV-Vis spectra of  $\text{Fe}^{3+}$  ions and complex **1** in aqueous solution were tested (Figure S5 in the ESI<sup>†</sup>). A wide absorption band of  $\text{Fe}^{3+}$  ions in aqueous solution in the range of 270–350 nm covered the absorption bands of complex **1** in water, indicating that there was an energy competition between the  $\text{Fe}^{3+}$  ions and the complex, which ultimately led to fluorescence quenching of the complex, as has been reported in other MOF literature [43–46].

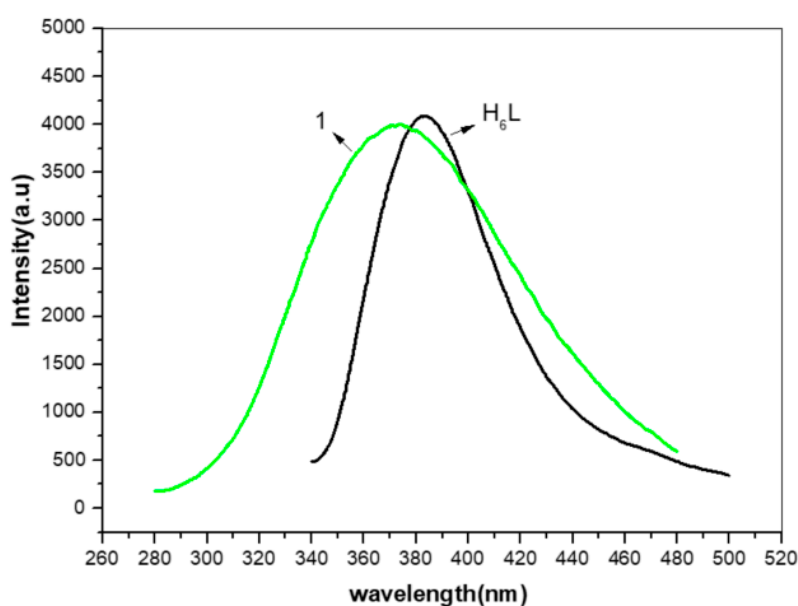


Figure 4. Solid-state emission spectra of **1**:  $\text{H}_6\text{L}$  at room temperature.

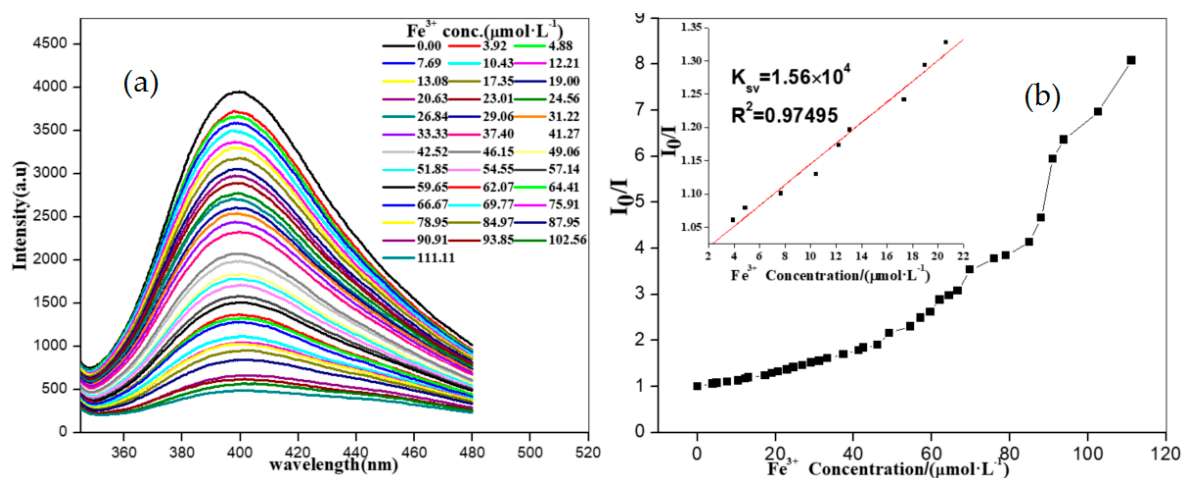


Figure 5. Stern–Volmer plot of **1** with 0.2 mM  $\text{Fe}^{3+}$  solution (a) and (b).



### 3.7. Electrochemical Properties

Subsequently, the electrochemical properties of **2** were studied. The bulk-modified carbon paste electrode (CPE) does not dissolve in water and common organic solvents, so we chose it. The **2**-modified CPE (**2**-CPE) was made with 2 mg graphite powder, 2 mg complex **2**, and the right amount of paraffin oil in an agate mortar for around half an hour to achieve even mixing. Then, it was added to a 3-mm inner diameter Teflon tube and connected to a copper wire to establish electrical contact. The cyclic voltammograms of the **2**-CPE in 0.5 mol·L<sup>-1</sup> NaOH solution are shown in Figure S6 (ESI<sup>†</sup>). It can be seen clearly that in the potential range of +400 to -800, a reversible redox peak is observed for **2**-CPE, which could be attributed to the redox of Cu(II)/Cu(I) [47].  $E_{1/2} = (E_{pa} + E_{pc})/2$  was -219.5 mV (50 mV/s) for **2**-CPE.

The scan rate's effect on the electrochemical behavior of **2**-CPE was investigated in 0.5 mol·L<sup>-1</sup> NaOH solution (Figure 6). At higher scan rates, the peak potentials changed gradually: the cathodic peak potentials shifted in a negative direction, and the homologous anodic peak potentials shifted in a positive direction. The inset of Figure 6 shows that the peak currents were proportional to the square root of the scan rates, suggesting that the redox processes for **2**-CPE are surface-controlled [48].

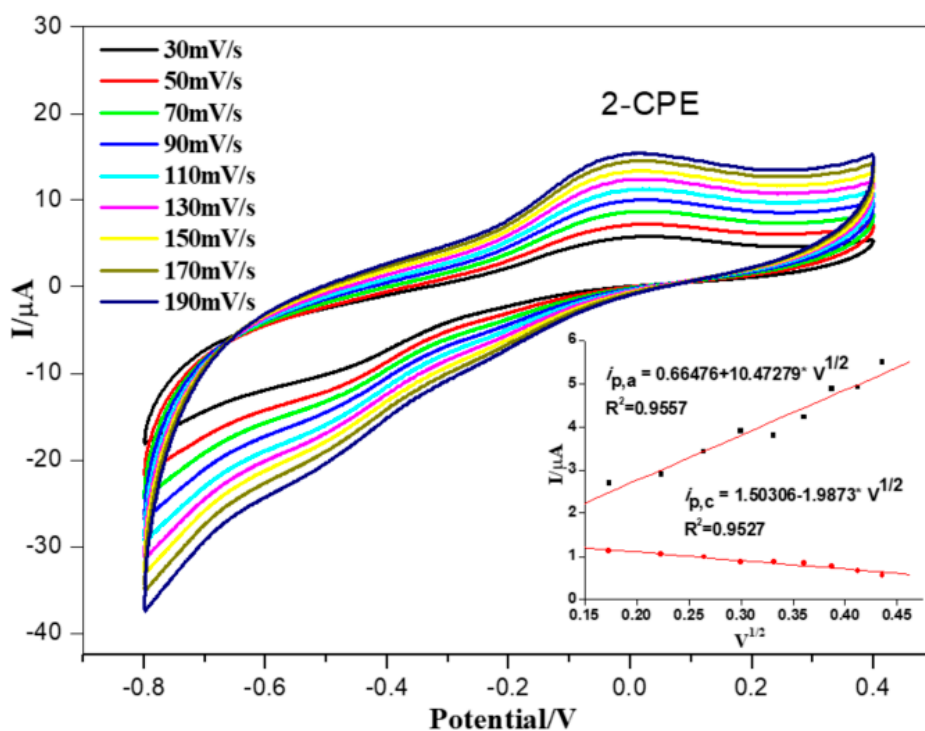


Figure 6. Cyclic voltammogram of **2**-CPE in 0.5M NaOH solution at 30 to 190 mV/s scan rates.

## 4. Conclusions

In summary, three complexes were synthesized with a hexacarboxylic acid ligand and nitrogen-containing ligands, and their PXRD, thermal stability, IR, luminescent, and electrochemical properties were also studied. In short, for **1**, adjacent Cd(II) ions were joined by carboxylic acid ligands L<sup>6-</sup> to form a 3D framework. Complex **1** had better photoluminescent properties, and it could be used as a potential fluorescence material for sensing Fe<sup>3+</sup> ions with high selectivity and sensitivity, where the  $K_{SV}$  was calculated to be  $1.56 \times 10^4$  M<sup>-1</sup>. For **2**, the Cu(II) ion was bonded to the carboxylic acid ligand L<sup>6-</sup> to form a 3D framework structure. For **3**, the Mn(II) ion and H<sub>3</sub>L<sup>3-</sup> ligands formed 1D chains, and then the 1D chains constituted a 2D layer by linking with bibp ligands. Finally, a 3D frame was obtained through layering. Furthermore, **2** might have potential applications in the field of electrochemistry due to its good redox performance.

**Supplementary Materials:** CCDC 1896443, 1896442, and 1959345 contain the supplementary crystallographic data for complexes 1–3, respectively. These data can be obtained free of charge from the Cambridge Crystallographic Data Center via [www.ccdc.cam.ac.uk/data\\_request/cif](http://www.ccdc.cam.ac.uk/data_request/cif). The following are available online at <http://www.mdpi.com/1420-3049/24/24/4431/s1>, Table S1: Selected Bond Lengths (Å) and Angles (deg) for compounds 1–3; Figure S1: Simulated (black), experimental (red), immersed in water after 2 days (blue) and immersed in Fe<sup>3+</sup> (0.01M) after 2 day (green) powder X-ray diffraction patterns of compound 1; Figure S2: Simulated (black), experimental (red) and immersed in water after 2 days (blue) powder X-ray diffraction patterns of compound 2; Figure S3: Simulated (black) and experimental (red) powder X-ray diffraction patterns of compound 3; Figure S4: The TGA diagrams of 1, 2 and 3; Figure S5: UV-Vis spectra of Fe<sup>3+</sup>, complex 1 in aqueous solution; Figure S6: CV of 2-CPE in 0.5 M NaOH solution at 50 mV/s.

**Author Contributions:** Conceptualization, L.Z. and L.M.; funding acquisition, L.Z.; project administration, L.Z.; investigation, G.G., X.L. and Z.L.; formal analysis, L.M., J.X. and X.Z.; writing—original draft, L.M.; writing—review and editing, all authors.

**Funding:** This research was funded by [Science and Technology Development Planning of Jilin Province, China] grant number [No. 20170101098JC] and by [the 13th Five Science and Technology Research of the Jilin Province Department of Education] grant number [No. JJKH20181174KJ].

**Acknowledgments:** The authors thank the technicians of Changchun Normal University for the technical support.

**Conflicts of Interest:** The authors declare no conflict of interest.

## References

1. Goswami, P.K.; Singh, M.; Thaimattam, R.; Ramanan, A. Extending the supramolecular synthon concept in flexible polyaminocarboxylate based coordination polymers. *CrystEngComm* **2013**, *15*, 9787–9797. [[CrossRef](#)]
2. Han, S.D.; Song, W.C.; Zhao, J.P.; Yang, Q.; Liu, S.J.; Lia, Y.; Bu, X.H. Synthesis and ferrimagnetic properties of an unprecedented polynuclear cobalt complex composed of [Co<sub>24</sub>] macrocycles. *Chem. Commun.* **2013**, *49*, 871–873. [[CrossRef](#)] [[PubMed](#)]
3. Gole, B.; Sanyal, U.; Banerjee, R.; Mukherjee, P.S. High Loading of Pd Nanoparticles by Interior Functionalization of MOFs for Heterogeneous Catalysis. *Inorg. Chem.* **2016**, *55*, 2345–2354. [[CrossRef](#)] [[PubMed](#)]
4. Amo-Ochoa, P.; Zamora, F. Coordination polymers with nucleobases: From structural aspects to potential applications. *Coord. Chem. Rev.* **2014**, *276*, 34–58. [[CrossRef](#)]
5. Zhou, H.C.; Kitagawa, S. Metal–Organic Frameworks (MOFs). *Chem. Soc. Rev.* **2014**, *43*, 5415–5418. [[CrossRef](#)] [[PubMed](#)]
6. Chen, X.; Liu, G. Double-Stranded Helices and Molecular Zippers Assembled from Single-Stranded Coordination Polymers Directed by Supramolecular Interactions. *Chem. Eur. J.* **2002**, *8*, 4811–4817. [[CrossRef](#)]
7. Akhbari, K.; Morsali, A. Modulating methane storage in anionic nano-porous MOF materials via post-synthetic cation exchange process. *Dalton Trans.* **2013**, *42*, 4786–4789. [[CrossRef](#)]
8. Keskin, S.; Sholl, D.S. Selecting metal organic frameworks as enabling materials in mixed matrix membranes for high efficiency natural gas purification. *Energy Environ. Sci.* **2010**, *3*, 343–351. [[CrossRef](#)]
9. Kuppler, R.J.; Timmons, D.J.; Fang, Q.R.; Li, J.R.; Makal, T.A.; Young, M.D.; Yuan, D.Q.; Zhao, D.; Zhuang, W.J.; Zhou, H.C. Potential applications of metal-organic frameworks. *Coord. Chem. Rev.* **2009**, *253*, 3042–3066. [[CrossRef](#)]
10. Jiang, J.; Yaghi, O.M. Bronsted Acidity in Metal–Organic Frameworks. *Cheminform* **2015**, *115*, 6966–6997. [[CrossRef](#)]
11. Hill, R.J.; Long, D.L.; Champness, N.R.; Hubberstey, P.R. New Approaches to the Analysis of High Connectivity Materials: Design Frameworks Based upon 4<sup>4</sup>- and 6<sup>3</sup>-Subnet Tectons. *Chem. Rev.* **2005**, *38*, 335–348. [[CrossRef](#)] [[PubMed](#)]
12. Li, H.Y.; Wei, Y.L.; Dong, X.Y.; Zang, S.Q.; Mak, T.C.W. Novel Tb-MOF Embedded with Viologen Species for Multi-Photofunctionality: Photochromism, Photomodulated Fluorescence, and Luminescent pH Sensing. *Chem. Mater.* **2015**, *27*, 1327–1331. [[CrossRef](#)]
13. Rhauderwiek, T.; Heidenreich, N.; Reinsch, H.; Øien-Ødegaard, S.; Lomachenko, K.A.; Rütt, U.; Soldatov, A.V.; Lillerud, K.P.; Stock, N. Co-ligand dependent Formation and Phase Transformation of Four Porphyrin-based Cerium MOFs. *Cryst. Growth Des.* **2017**, *17*, 3462–3474. [[CrossRef](#)]

14. Li, M.; Li, D.; O’Keeffe, M.; Yaghi, O.M. Topological Analysis of Metal–Organic Frameworks with Polytopic Linkers and/or Multiple Building Units and the Minimal Transitivity Principle. *Chem. Rev.* **2014**, *114*, 1343–1370. [[CrossRef](#)]
15. Wang, X.S.; Chrzanowski, M.; Kim, C.; Gao, W.Y.; Wojtas, L.; Chen, Y.S.; Zhanga, X.P.; Ma, S. Quest for highly porous metal–metalloporphyrin framework based upon a custom-designed octatopic porphyrin ligand. *Chem. Commun.* **2012**, *48*, 7173–7175. [[CrossRef](#)]
16. Chen, Z.; Mi, X.; Lu, J.; Wang, S.; Li, Y.; Doua, J.; Lia, D. From 2D→3D interpenetration to packing: N coligand-driven structural assembly and tuning of luminescent sensing activities towards Fe<sup>3+</sup> and Cr<sub>2</sub>O<sub>7</sub><sup>2-</sup> ions. *Dalton Trans.* **2018**, *47*, 6240–6249. [[CrossRef](#)]
17. Feng, X.; Feng, Y.Q.; Guo, N.; Sun, Y.L.; Zhang, T.; Ma, L.F.; Wang, L.Y. Series d–f Heteronuclear Metal–Organic Frameworks: Color Tunability and Luminescent Probe with Switchable Properties. *Inorg. Chem.* **2017**, *56*, 1713–1721. [[CrossRef](#)]
18. Zheng, T.T.; Zhao, J.; Fang, Z.W.; Li, M.T.; Sun, C.Y.; Li, X.; Wang, X.L.; Su, Z.M. A luminescent metal organic framework with high sensitivity for detecting and removing copper ions from simulated biological fluids. *Dalton Trans.* **2017**, *46*, 2456–2461. [[CrossRef](#)]
19. Chen, S.G.; Shi, Z.Z.; Qin, L.; Jia, H.L.; Zheng, H.G. Two New Luminescent Cd(II)-MOFs as Bi-functional Chemosensors for Detection of Cations Fe<sup>3+</sup>, Anions CrO<sub>4</sub><sup>2-</sup> and Cr<sub>2</sub>O<sub>7</sub><sup>2-</sup> in Aqueous Solution. *Cryst. Growth. Des.* **2017**, *17*, 67. [[CrossRef](#)]
20. Hyman, L.; Franz, K. Probing oxidative stress: Small molecule fluorescent sensors of metal ions, reactive oxygen species, and thiols. *Coord. Chem. Rev.* **2012**, *256*, 2333–2356. [[CrossRef](#)]
21. Yi, F.Y.; Yang, W.; Sun, Z.M. Highly selective acetone fluorescent sensors based on microporous Cd(ii) metal–organic frameworks. *J. Mater. Chem.* **2012**, *22*, 23201–23209. [[CrossRef](#)]
22. Hua, J.A.; Zhao, Y.; Kang, Y.S.; Lu, Y.; Sun, W.Y. Solvent-dependent zinc(II) coordination polymers with mixed ligands: Selective sorption and fluorescence sensing. *Dalton Trans.* **2015**, *44*, 11524–11532. [[CrossRef](#)] [[PubMed](#)]
23. Wen, G.X.; Wu, Y.P.; Dong, W.W.; Zhao, J.; Li, D.S.; Zhang, J. An Ultrastable Europium(III)–Organic Framework with the Capacity of Discriminating Fe<sup>2+</sup>/Fe<sup>3+</sup> Ions in Various Solutions. *Inorg. Chem.* **2016**, *55*, 10114–10117. [[CrossRef](#)] [[PubMed](#)]
24. Barba-Bon, A.; Costero, A.M.; Gil, S. A new selective fluorogenic probe for trivalent cations. *Chem. Commun.* **2012**, *48*, 3000–3002. [[CrossRef](#)] [[PubMed](#)]
25. Hu, F.L.; Shi, Y.X.; Chen, H.H.; Lang, J.P. A Zn(II) coordination polymer and its photocycloaddition product: Syntheses, structures, selective luminescence sensing of iron(III) ions and selective absorption of dyes. *Dalton Trans.* **2015**, *44*, 18795–18803. [[CrossRef](#)] [[PubMed](#)]
26. Yang, W.; Tian, W.G.; Liu, X.X.; Wang, L.; Sun, Z.M. Syntheses, Structures, Luminescence, and Photocatalytic Properties of a Series of Uranyl Coordination Polymers. *Cryst. Growth Des.* **2014**, *14*, 5904–5911. [[CrossRef](#)]
27. Wang, J.; Jiang, M.; Yan, L.; Peng, R.; Huangfu, M.J.; Guo, X.X.; Li, Y.; Wu, P.Y. Multifunctional Luminescent Eu(III)-Based Metal–Organic Framework for Sensing Methanol and Detection and Adsorption of Fe(III) Ions in Aqueous Solution. *Inorg. Chem.* **2016**, *55*, 12660–12668. [[CrossRef](#)]
28. Wang, J.; Wang, J.R.; Li, Y.; Jiang, M.; Zhang, L.W.; Wu, P.Y. A europium(III)-based metal–organic framework as a naked-eye and fast response luminescence sensor for acetone and ferric iron. *New J. Chem.* **2016**, *40*, 8600–8606. [[CrossRef](#)]
29. Hao, Z.M.; Yang, G.C.; Song, X.Z.; Zhu, M.; Meng, X.; Zhao, S.N. A europium(III) based metal–organic framework: Bifunctional properties related to sensing and electronic conductivity. *J. Mater. Chem. A* **2014**, *2*, 237–244. [[CrossRef](#)]
30. Liang, Y.T.; Yang, G.P.; Liu, B.; Yan, Y.T.; Xi, Z.P.; Wang, Y.Y. Four super water-stable lanthanide–organic frameworks with active uncoordinated carboxylic and pyridyl groups for selective luminescence sensing of Fe<sup>3+</sup>. *Dalton Trans.* **2015**, *44*, 13325–13330. [[CrossRef](#)]
31. Zhang, J.N.; Lu, H.B.; Yan, C.; Yang, Z.B.; Zhu, G.Q.; Gao, J.Z.; Yin, F.; Wang, C.L. Fabrication of conductive graphene oxide-WO<sub>3</sub> composite nanofibers by electrospinning and their enhanced acetone gas sensing properties. *Sens. Actuators B.* **2018**, *264*, 128–138. [[CrossRef](#)]
32. Bricks, J.L.; Kovalchuk, A.; Trieflinger, C.; Nofz, M.; Büschel, M.; Tolmachev, A.I.; Daub, J.; Rurack, K. On the Development of Sensor Molecules that Display Fe(III)-amplified Fluorescence. *J. Am. Chem. Soc.* **2005**, *127*, 13522–13529. [[CrossRef](#)] [[PubMed](#)]

33. Li, S.; Song, J.; Ni, C.; Wang, Z.N.; Gao, X.; Shi, Z.; Bai, F.Y.; Xing, Y.H. Photoelectric properties and potential nitro derivatives sensing by a highly luminescent of Zn (II) and Cd (II) metal-organic frameworks assembled by the flexible hexapodal ligand, 1,3,5-triazine-2,4,6-triamine hexaacetic acid. *RSC Adv.* **2016**, *6*, 36000–36010. [[CrossRef](#)]
34. Song, J.; Gao, X.; Wang, Z.N.; Li, C.R.; Xu, Q.; Bai, F.Y.; Shi, Z.F.; Xing, Y.H. Multifunctional Uranyl Hybrid Materials: Structural Diversities as a Function of pH, Luminescence with Potential Nitrobenzene Sensing, and Photoelectric Behavior as p-type Semiconductors. *Inorg. Chem.* **2015**, *54*, 9046–9059. [[CrossRef](#)] [[PubMed](#)]
35. Yang, B.; Chen, N.; Tse, K.M.; Lee, H.P. Hydrothermal synthesis, crystal structures, and luminescent properties of two cadmium(ii) coordination polymers based on dicarboxylate and imidazole-containing coligands. *Z. Anorg. Allg. Chem.* **2015**, *641*, 601–605. [[CrossRef](#)]
36. Li, X.C.; Zheng, J.; He, C.J.; Wang, K.; Chai, W.W.; Duan, Y.T.; Tang, B.J.; Rui, Y.C. MOF-derived Cu–C loaded with SnO<sub>x</sub> as a superior anode material for lithium-ion batteries. *Electrochim. Acta* **2019**, *326*, 134960. [[CrossRef](#)]
37. Rambabu, D.; Ashraf, M.; Pooja, G.A.; Dhir, A. Mn-MOF@Pi composite: Synthesis, characterisation and an efficient catalyst for the Knoevenagel condensation reaction. *Tetrahedron Lett.* **2017**, *58*, 4691–4694. [[CrossRef](#)]
38. Meng, L.S.; Zhao, L.; Zhao, C.J.; Lin, X. Synthesis, characterization and electrochemical properties of two metal cobalt complexes constructed by tetradentate carboxylic. *J. Mol. Struct.* **2019**, *1179*, 425–430. [[CrossRef](#)]
39. Sheldrick, G.M. SHELXT–Integrated space-group and crystal-structure determination. *Acta Crystallogr.* **2008**, *64*, 112–122. [[CrossRef](#)]
40. Huang, F.P.; Yang, Z.M.; Yao, P.F.; Yu, Q.; Tian, J.L.; Bian, H.D.; Yan, S.P.; Liao, D.Z.; Cheng, P. Coordination assemblies of the CdII–BDC/bpt mixed-ligand system: Positional isomeric effect, structural diversification and luminescent properties. *CrystEngComm* **2013**, *15*, 2657–2688. [[CrossRef](#)]
41. Su, Y.; Zhang, S.; Li, Y.; Zhu, A.Z.; Meng, Q. Four d<sup>10</sup> Metal Coordination Polymers Containing IsomericThiodiphtalic Ligands: Crystal Structures and LuminescentProperties. *Cryst. Growth Des.* **2007**, *7*, 1277–1283. [[CrossRef](#)]
42. Thomas, S.W.; Joly, G.D.; Swager, T.M. Chemical sensors based on amplifying fluorescent conjugated polymers. *Chem. Rev.* **2007**, *107*, 1339–1386. [[CrossRef](#)] [[PubMed](#)]
43. Zhang, S.T.; Yang, J.; Wu, H.; Liu, Y.Y.; Ma, J.F. Systematic investigation of high-sensitivity luminescent sensing for polyoxometalates and Iron(III) by MOFs assembled with a new resorcin[4]arene-functionalized tetracarboxylate. *Chem. Eur. J.* **2015**, *21*, 15806–15819. [[CrossRef](#)] [[PubMed](#)]
44. Zhou, J.M.; Shi, W.; Li, H.M.; Li, H. Experimental studies and mechanism analysis of high-sensitivity luminescent sensing of pollutional small molecules and ions in Ln<sub>4</sub>O<sub>4</sub> cluster based microporous metal-organic framework. *J. Phys. Chem. C* **2014**, *118*, 416–426. [[CrossRef](#)]
45. Zhao, X.L.; Tian, D.; Gao, Q.; Sun, H.W. A chiral lanthanide metal-organic framework for selective sensing of Fe(III) ion. *Dalton Trans.* **2016**, *45*, 1040–1046. [[CrossRef](#)]
46. Das, D.; Biradha, K. Luminescent Coordination polymers of naphthalene based diamide with rigid and flexible dicarboxylates: Sensing of nitro explosives, Fe(III) Ion, and dyes. *Cryst. Growth Des.* **2018**, *18*, 3683–3692. [[CrossRef](#)]
47. Salimi, A.; Alizadeh, V.; Hadadzadeh, H. Renewable Surface Sol-gel Derived Carbon Ceramic Electrode Modified with Copper Complex and Its Application as an Amperometric Sensor for Bromate Detection. *Electroanalysis* **2004**, *16*, 1984–1991. [[CrossRef](#)]
48. Wang, X.L.; Mu, B.; Lin, H.Y.; Liu, G.C. Three new two-dimensional metal-organic coordination polymers derived from bis(pyridinecarboxamide)-1,4-benzene ligands and 1,3-benzenedicarboxylate: Syntheses and electrochemical property. *J. Organomet. Chem.* **2011**, *696*, 2313–2321. [[CrossRef](#)]

